Geochimica et Cosmochimica Acta, Vol. 69, No. 3, pp. 541–552, 2005

0016-7037/05 $30.00 + .00

doi:10.1016/j.gca.2004.07.009

Adsorption of oxalate and malonate at the water-goethite interface: molecular surface speciation from IR spectroscopy

Per Persson* and Kristina Axe

Department of Chemistry, Inorganic Chemistry, Umeå University, SE-901 87 Umeå, Sweden

(*Received January* 27, 2004; *accepted in revised form July* 8, 2004)

Abstract—The adsorption of oxalate and malonate at the water-goethite interface was studied as a function of pH and total ligand concentrations by means of quantitative adsorption measurements and attenuated total reflectance Fourier transform infrared spectroscopy. The obtained results conclusively showed that oxalate and malonate both form outer-sphere and inner-sphere surface complexes on goethite, and that these complexes coexist over a broad pH interval. The inner-sphere complexes were favored by low pH, while the relative concentrations of the outer-sphere species increase with increasing pH. Based on comparisons with model complexes characterized by Extended X-Ray Adsorption Fine Structure (EXAFS) and results from theoretical frequency calculations, the structures of the inner-sphere complexes of oxalate and malonate were best described as mononuclear five- and six-membered ring chelate structures, respectively. The stability of the inner-sphere complexes followed the trend expected from solutions studies, with the oxalate five-membered ring yielding the more stable complexes compared to the six-membered ring of malonate. The increased stability of the inner-sphere complex of oxalate was manifested in a greater extent of adsorption at acidic pH values. Despite the fact that significant amounts of oxalate and malonate inner-sphere surface complexes were formed, no ligand-promoted dissolution was observed at the experimental conditions in the study.

1. INTRODUCTION

Interactions between particle surfaces and organic matter containing carboxylic acid groups influence many processes in natural waters and soils (Stumm, 1992). Some examples are (i) the dissolution of mineral particles and the subsequent release of important micronutrients; (ii) the transport of metal ions; and (iii) the bioavailability of both natural and anthropogenic chemicals. In several cases, molecular-based hypotheses have been proposed to explain the role of organic acids in these and other processes (for example Bell and Palmer, 1994; Bennett and Casey, 1994; Drever and Vance, 1994), but due to the lack of fundamental molecular information, they often have not been verified or falsified. It is in this context that detailed studies of model systems are of significant value, since they provide means to characterize the composition and structure of the surface species and their reactivity. This information can, in turn, be used to test the formulated hypotheses.

The quantitative adsorption of carboxylates to mineral surfaces has been characterized for many ligand-mineral systems (e.g., Kummert and Stumm, 1980; Balistrieri and Murray, 1987; Mesuere and Fish, 1992; Ali and Dzombak, 1996; Filius et al., 1997). Several studies also have been devoted to the molecular adsorption mechanisms, the structures of the surface complexes formed, and the reactivity of these species (Parfitt et al., 1977; Yost et al., 1990; Tejedor-Tejedor et al., 1992; Hug and Sulzberger, 1994; Nordin et al., 1997; Dobson and McQuillan, 1999; Kubicki et al., 1999; Boily et al., 2000; Duckworth and Martin, 2001; Hind et al., 2001). In most previous studies, the adsorption of carboxylates has been explained either by the formation of inner-sphere or outer-sphere surface complexes. Inner sphere implies a direct bond between the carboxylate and a surface metal ion, while in outer-sphere complexes no such bond exists, and instead the dominating driving force of formation is the attraction between the positively charged surface and the negatively charged carboxylate. In some recent investigations, however, inner-sphere and outer-sphere complexes of benzenecarboxylates have been found to coexist on metal (hydr)oxide surfaces (Nordin et al., 1997; Boily et al., 2000). The structures of these ligands, together with spectroscopic information, indicated mononuclear inner-sphere complexes where one oxygen from each of two carboxylate groups coordinated to a surface metal ion forming a seven-membered ring chelate structure. From solution studies, it is known that for metal ions such as Fe(III), seven-membered rings yield comparatively weak complexes, while six- and five-membered rings generally result in progressively more stable complexes (Martell and Hancock, 1996). An important question is if and how such differences in ligand structure also significantly influence the adsorption reactions, and in particular the bonding mechanisms between the ligand and the surface.

In this respect, the adsorption of oxalate ($C_2O_4^{2-}$) and malonate ($H_2C_3O_4^{2-}$) onto mineral surfaces is of particular interest. Apart from being suitable model compounds for dicarboxylates capable of forming five- and six-membered ring chelate structures, both ligands also occur and play important roles in aquatic systems and in soils. In previous studies of oxalate and malonate adsorption to Fe(III) (hydr)oxide mineral surfaces, different surface structures have been suggested. However, in almost all cases adsorption was explained by inner-sphere surface complexation mechanisms. Modeling adsorption data, Filius et al. (1997) suggested the presence of one oxalate and three different malonate inner-sphere complexes at the goethite surface. All were assigned bidentate structures involving only

* Author to whom correspondence should be addressed (Per.Persson@chem.umu.se).

Table 1. The dominating species of the oxalate and malonate solutions analyzed by EXAFS and IR spectroscopy. Compositions calculated using constants from (Smith and Martell, 1982).

Analyzed Species	$[L_{tot}]$ (mM)	$[Fe_{tot}]$ (mM)	pH	$[H_2L]$ (mM)	$[HL^-]$ (mM)	$[L^{2-}]$ (mM)	$[Fe^{3+}]$ (aq) (mM)	$[FeL^+]$ (mM)	$[FeL_2^-]$ (mM)	$[FeL_3^{3-}]$ (mM)
IR solutions										
$H_2C_2O_4$	100.0		1.2	40.0	60.0					
HC_2O_4	100.0		2.2	5.9	90.0	4.0				
C_4^{2-}	100.0		7.3			100				
$Fe(C_2O_4)^+$	30.0	30.0	1.5				3.9	20.3	4.0	
$Fe(C_2O_4)_3^{3-}$	90.0	30.0	4.0		0.2				0.7	29.3
$H_4C_3O_4$	20.0		1.0	19.6	0.4					
$H_3C_3O_4$	20.0		3.7	1.3	17.9	0.8				
$H_2C_3O_4^{2-}$	20.0		8.5			20				
$Fe(H_2C_3O_4)^+$	15.0	30.0	1.8	0.4	0.1		11.7	13.9	0.3	
$Fe(H_2C_3O_4)_3^{3-}$	95.0	30.0	4.4	0.1	7.2	1.5			3.9	26.1
EXAFS solutions										
$Fe(C_2O_4)_3^{3-}$	90.0	30.0	4.0						0.8	29.2
$Fe(H_2C_3O_4)_3^{3-}$	175.0	40.0	5.6						0.4	39.6

one of the carboxylate groups. On the surface of hematite, Duckworth and Martin (2001) from IR spectroscopic results concluded mononuclear five-membered and six-membered ring chelates involving both carboxylate groups for oxalate and malonate, respectively, as the only surface species. Also using IR spectroscopy, Lenhart et al. (2001), on the other hand, suggest the formation of two or more surface species on hematite, of which at least one is an inner-sphere complex. From these few examples it is clear there is disagreement in the literature concerning how oxalate and malonate bind to surfaces of iron (hydr)oxides.

The present study was designed to further investigate the molecular speciation of oxalate and malonate adsorbed onto an Fe(III) (hydr)oxide mineral surface. To accomplish this, adsorption of oxalate and malonate on goethite were studied over a wide range of chemical conditions, varying pH, total ligand concentration, and time. Each sample was characterized at both macroscopic and molecular levels. Total adsorption and the potential release of iron into solution were measured with classical wet-chemical techniques, and the molecular-level surface speciation was investigated by in situ IR spectroscopy. To facilitate the interpretation of the IR spectra obtained, these were compared with spectra of model species in solution and with theoretical frequencies obtained from molecular orbital calculations. The structures of the aqueous Fe(III) model complexes with oxalate and malonate were characterized by means of extended X-ray absorption fine structure (EXAFS) spectroscopy.

2. EXPERIMENTAL

2.1. Chemicals and Solutions

The synthesis and characterization of the goethite particles have been described in detail by Lützenkirchen et al. (2002). Briefly, goethite (α-FeOOH) was prepared in polyethylene bottles by adding 2.5 L of 2.5 M KOH (EKA p.a.) to 10 L of 0.15 M $Fe(NO_3)_3$ (Merck p.a.) at a rate of 10 mL/min. The precipitates were aged for 48 h at 80°C and dialyzed for two weeks. The resulting particles were identified to be goethite by X-ray powder diffraction. The N_2 BET surface area was determined to 84 m^2/g. The suspension was diluted to a concentration of 10.8 g/L and NaCl added to an ionic strength of 0.1 M before used in the adsorption experiments.

For all experimental work, deionized water (Milli-Q Plus) boiled for 45 min to remove dissolved CO_2, was used. pH adjustments were accomplished with NaOH (0.5 or 0.1 M) and HCl (0.1 M). Sodium chloride (Merck p.a.) was dried at 180°C and used to obtain a total chloride concentration of 0.1 M in all solutions and suspensions used. Ligand solutions were prepared by dissolving weighed amounts of disodium oxalate ($Na_2C_2O_4$, Merck, p.a.) and malonic acid ($C_3H_4O_4$, Merck, p.a.).

For the adsorption experiments, the ligand solutions were spiked with the ^{14}C isotope of oxalic and malonic acid (Amersham International) to obtain a total activity of ~300 Bq/ml of suspension. For quantitative analysis, the scintillation cocktail Optiphase "High Safe 3" (Wallac) was used.

Solutions of H_2L, HL^-, L^{2-}, FeL^+, and FeL_3^{3-} ($L^{2-} = C_2O_4^{2-}$ or $H_2C_3O_4^{2-}$) were prepared for the collection of EXAFS and IR spectra. To obtain solutions containing predominantly one species, model calculations using the chemical speciation program SOLGASWATER (Eriksson, 1979) were performed. Stability constants were taken from Smith and Martell (1982). The compositions of the solutions are summarized in Table 1. For the determination of the IR molar absorption coefficients for L^{2-} (aq) and FeL^+ (aq), solutions in the range 5 to 20 mM were prepared.

2.2. Adsorption Experiments

The pH dependence of ligand adsorption was studied in series of batch experiments in the pH range 2.5 to 8. Four series were carried out at total malonate concentrations of 0.6, 0.7, 0.8, and 1.4 $\mu mol/m^2$, and two series at total oxalate concentrations of 0.7 and 1.4 $\mu mol/m^2$. The goethite suspension was acidified to pH ~5, and purged with Ar (g) overnight before use. Five ml of suspension was placed in 10 mL polypropylene centrifuge tubes and different amounts of 0.1 M NaOH or HCl was added to get an even distribution of pH values. pH was measured with a combination pH electrode (Ross). The outer reference cell was filled with 0.1 M NaCl and calibrated with solutions of known [H+], which means that pH corresponds to $-\log[H^+]$ and not to $-\log(a_H^+)$. Ligands solutions spiked with the ^{14}C isotope were added, and the samples were left to react on an end-over-end rotator for 24 ± 1 h after which pH was measured. The samples were centrifuged at 4500 rpm for 10 min, after which some of the supernatant was used for immediate IR analysis. 2.25 mL of supernatant was transferred into a new centrifuge tube and centrifuged for a further 20 min, from which solution for dissolved iron and ligand analyses were taken. A small

Table 2a. Experimental IR frequencies and tentative assignments of the main peaks of oxalate and protonated oxalate species in the frequency region 1200–1800 cm^{-1}.

Assignment	$C_2O_4^{2-}$	$HC_2O_4^-$	$H_2C_2O_4$
$\nu_{C=O}$	—	1728	1735
ν_{C-O}^{as}	1569	1609	—
ν_{C-O}^{s}	1308	1307	—
ν_{C-OH}	—	1242	1233

volume of supernatant was left to cover the mineral paste until used for IR analysis, which was started within 20 min of sample collection.

Adsorption experiments as a function of time were carried out at constant pH using an ABU 901 pH stat controller connected to an ABU 302 burette filled with 0.1 M HCl and a combination pH electrode (Ross). Again the outer reference cell of the electrode was filled with 0.1 M NaCl and calibrated with solutions of known $[H^+]$. The goethite suspension (initial volume 75 mL) was adjusted to the required pH and purged with Ar(g) for at least 16 h to remove any dissolved CO_2 before the ligand solution was added. After different reaction times (from a few min to 48 h), 5 mL sample aliquots were removed into 10 mL polypropylene centrifuge tubes. The samples were immediately centrifuged and the procedure described above was followed.

2.3. Analysis

For iron analysis, duplicate samples were acidified to pH below 2 with concentrated HCl (analytical grade). Total iron was measured using flame atomic absorption spectrometry (Perkin-Elmer AAS 3110). However no significant dissolution of goethite was detected; all samples were around or below the detection limit 2 μM $[Fe]_{tot}$. Accordingly, at the experimental conditions studied herein no ligand-promoted dissolution was observed.

Liquid scintillation counting (LSC) was used to determine the concentration of ligand in the supernatant. For analysis, 0.5 mL of the supernatant was thoroughly mixed with 3 mL of Optiphase "High Safe 3" (Wallac) scintillation liquid. The samples were kept in the dark overnight before being analyzed using a Beckman LS6500 Multipurpose scintillation counter. The difference between the total activity added and the one detected in the supernatant was assumed to be directly proportional to the amount of ligand adsorbed onto the goethite particles. At high pH, where no adsorption takes place, full recovery of the radioactivity added was observed showing that there was no problem with ligand adsorption to the walls of the reaction vials or the centrifuge tubes during sample handling. The reproducibility was tested separately using a typical setup. Results within 2% were obtained for repeating the same experiment as well as quadruple replicate analysis of each repeat.

2.4. Attenuated Total Reflectance Fourier Transform Infrared (ATR-FTIR) Spectroscopy

The IR spectra were collected with a Perkin-Elmer Spectrum 2000 FTIR spectrometer equipped with a deuterated triglycine sulfate (DTGS) detector. All adsorption samples were analyzed as wet pastes with the ATR-FTIR technique. The spectra were recorded with a horizontal ATR accessory and a diamond/KRS5 material as the reflection element (SensIR Technologies). The angle of incidence for this setup is ~45°, which is far from the critical angle (ca. 30°). This, together with the fact that only peaks with low intensities are analyzed and that these do not overlap with stronger peaks (except for the asymmetric C-O stretch which overlaps with the intense H_2O bend), indicates that the effects of possible distortions known to occur in ATR spectra are minimized (Urban, 1996). The IR samples were prepared according to the procedure for the adsorption samples described above. After collecting the spectra of the empty cell and the supernatant, the wet paste was uniformly applied directly onto the diamond crystal and data were collected. During data collection, a quartz lid was placed over the ATR crystal and pressed tightly against a rubber gasket, ensuring no contact between the quartz lid and the sample. This sealed the sample from the atmosphere during data collection. For each spectrum, 100 scans were collected at a resolution of 4 cm^{-1}. The time from sampling of the suspension to completion of the paste spectrum was 30 to 35 min.

The raw spectrum of the wet paste is dominated by the strong absorptions between 1900 and 2600 cm^{-1} from the type II diamond and by the strong contributions from water. Therefore, to isolate the spectrum of ligand at the water-goethite interface, a subtraction procedure was necessary, of which the most critical step is to correctly remove the 1638 cm^{-1} water peak originating from the bending motion of bulk water. The empty cell spectrum was first subtracted from the supernatant and wet paste spectra, after which the resulting supernatant spectrum was subtracted from the corresponding paste spectrum. In this step, the subtraction of the 1638 cm^{-1} water peak was accomplished by using an appropriate subtraction factor of the supernatant spectrum. In this study, the factor varied between 0.97 and 1.0. Finally, the spectrum of goethite with no ligand present was subtracted to facilitate and minimize errors (or to further enhance the signal of the adsorbed organic ligand over the bulk mineral) in the quantitative peak evaluation. An important part of this work was also to study the solution complexes. To isolate IR spectra of ligand and iron-ligand species in the aqueous solutions, a similar procedure was followed, but for subtraction of the water contribution a spectrum of 0.1 M NaCl of matching pH was used.

Since ligand and iron-ligand species are present not only on the mineral surface but also in the aqueous phase, there is a possibility of interference from the species in solution, particularly at high pH when little ligand is adsorbed. In the experiments performed in this study, however, the highest total ligand concentrations were 1.2 mM, which is at the detection limit for these species with the ATR-FTIR technique and the experimental setup used in this study. The reason why we observe ligands at the interface is due to the adsorption, which significantly increases the "effective ligand concentration" in the paste. The supernatant spectra were checked for contributions from the ligand, and in all spectra presented, the ligand peak intensities were less than 5% of the intensities in the paste spectra. This contribution is further reduced by the subtraction procedure.

2.5. Extended X-Ray Absorption Fine Structure (EXAFS) Spectroscopy

2.5.1. EXAFS measurements

Fe K-edge EXAFS data were measured at the Stanford Synchrotron Radiation Laboratory, California on beam line 4-1. The ring energy was 3.0 GeV with ring currents between 60 and 100 mA. A Si(220) double crystal monochromator was used and detuned 50% to eliminate higher order harmonics. The incoming and transmitted beam was registered using ion chambers filled with N_2. The data were collected at room temperature in the fluorescence mode, with a Lytle detector filled with Ar gas. A Mn 6 μx filter and Soller slit setup were used to reduce Kβ fluorescence and scattering contributions to the signal. Internal calibration was performed by simultaneously measuring spectra from an Fe foil in transmission mode, throughout the duration of all scans. Six scans were collected per sample.

Table 2b. Experimental IR frequencies and tentative assignments of the main peaks of malonate and protonated malonate species in the frequency region 1200–1800 cm^{-1}.

Assignment	$H_2C_3O_4^{2-}$	$H_3C_3O_4^-$	$H_4C_3O_4$
$\nu_{C=O}$	—	1725	1730
$\nu_{C-O}^{as} + \delta_{CCH}$	1564	1576	—
δ_{CCH}	1438	1463	1464
$\nu_{C-O}^{s} + \delta_{CCH}$	1409	1412	—
$\nu_{C-O}^{s} + \delta_{CCH}$	1357	1372	—
δ_{CCH}	1258	1257	—
ν_{C-OH}	—	1274, 1168	1220, 1172

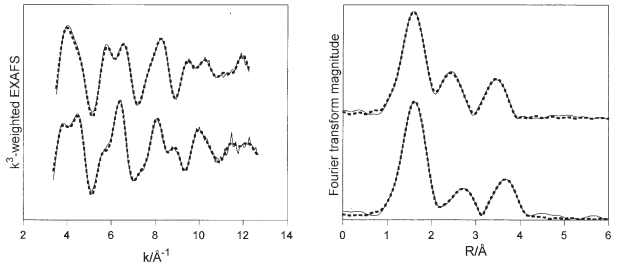

Fig. 1. k^3-weighted EXAFS spectra (left) of $Fe(C_2O_4)_3^{3-}$ (aq) (top) and $Fe(H_2C_3O_4)_3^{3-}$ (aq) (bottom), and the Fourier transformed data (right) of $Fe(C_2O_4)_3^{3-}$ (aq) (top) and $Fe(H_2C_3O_4)_3^{3-}$ (aq) (bottom). Experimental data are described by solid lines and the fit results with broken lines.

2.5.2. *EXAFS data treatment*

The EXAFS data were energy-calibrated and averaged with EXAFSPAK (George, 1995), and further analyzed using WinXAS (Ressler, 1998). Standard procedures were used for preedge subtraction, data normalization, and spline removal. The k^3-weighted EXAFS oscillations were Fourier transformed over the k-range 3.3 to 14.5 $Å^{-1}$ using a Bessel window function. The resulting Fourier transforms were used in the least-squares refinements, thus all results presented herein were obtained from R-space fits. Theoretical phase and amplitude functions, used in the refinements, for single and multiple scattering paths within assumed molecular models were calculated with the ab initio code FEFF7 (Ankudinov et al., 1998). The input structure was that obtained from the molecular orbital calculations and geometry optimizations of $Fe(C_2O_4)_3^{3-}$ and $Fe(H_2C_3O_4)_3^{3-}$ (see the paragraph below). Since the EXAFS amplitude is proportional to the coordination number and the amplitude reduction factor, S_0^2, the EXAFS spectrum of an acidic solution of iron(III) nitrate, where the Fe-O coordination number of $Fe(H_2O)_6^{3+}$ is known to be 6 (Johansson, 1992), was used to refine S_0^2. This value was found to be close to one, with the phase and amplitude functions for the Fe-O scattering path obtained from the FEFF calculation of $Fe(H_2C_3O_4)_3^{3-}$, and was set to one during the refinements of the EXAFS spectra.

2.6. Molecular Orbital Calculations

Theoretical vibration frequencies of the geometry optimized $Fe(C_2O_4)_3^{3-}$ and $Fe(H_2C_3O_4)_3^{3-}$ complexes were calculated with the density functional theory (DFT) using the hybrid functionals B3LYP. The standard 6-31+G* basis set was used in all calculations, and they were run with iron in its high-spin state ($s = 6$). No attempts were made to account for solvation effects. The calculations were performed with the program Gaussian 98 by Gaussian Inc., Pittsburgh, Pennsylvania USA (Frisch et al., 2001), and visualization of the calculated vibrational modes was accomplished with HyperChem v. 5 by Hypercube, Gainesville, Florida USA. The potential energy minimum structures of the complexes were obtained without applying symmetry restrictions; i.e., all bond lengths, angles, and dihedral angles were allowed to vary. The vibrational frequencies were calculated for the optimized structures and only real frequencies were obtained, which show that these structures represent minima at the potential energy surface.

3. RESULTS AND DISCUSSION

3.1. Structure and IR Spectra Of Aqueous Fe(III) Complexes with Oxalate and Malonate

A way to assess the structures of the oxalate and malonate surface complexes is by comparing their characteristic IR features to those of aqueous model complexes. This method relies on the fact that the IR characteristics of the ligands are very much determined by local chemical interactions, and thus, if the local chemical environments are similar in solution and at the surface, practically identical IR spectra are expected. With this approach the IR spectra-structure relationships for the model complexes need to be known. For aqueous oxalate and malonate, and protonated species thereof, the IR spectra have been previously discussed and assigned, and this information is summarized in Tables 2a and 2b (Cabaniss et al., 1998; Axe and Persson, 2001; Rosenqvist et al., 2003). To establish such relationships and to assign the IR spectra of aqueous Fe(III) complexes with oxalate and malonate also, the local structures around Fe(III) in $Fe(C_2O_4)_3^{3-}$ and $Fe(H_2C_3O_4)_3^{3-}$ were characterized by means of EXAFS spectroscopy. Once these structures were known, the experimental IR spectra could be assigned by calculating the theoretical frequencies of these structures using ab initio quantum chemical methods.

The k^3-weighted EXAFS spectra and the Fourier transformed data of $Fe(C_2O_4)_3^{3-}$ and $Fe(H_2C_3O_4)_3^{3-}$ are shown in Figure 1. By comparison with other oxalate and malonate complexes (Clausén et al., 2003), the most likely coordination geometries are chelate structures where one oxygen from each carboxylate group binds to Fe(III), forming five- and six-membered rings, respectively. Therefore, the chelate structures of $Fe(C_2O_4)_3^{3-}$ and $Fe(H_2C_3O_4)_3^{3-}$ (Fig. 2) obtained from the DFT geometry optimizations were used as input to FEFF7 to calculate the dominant scattering paths and to obtain phase and

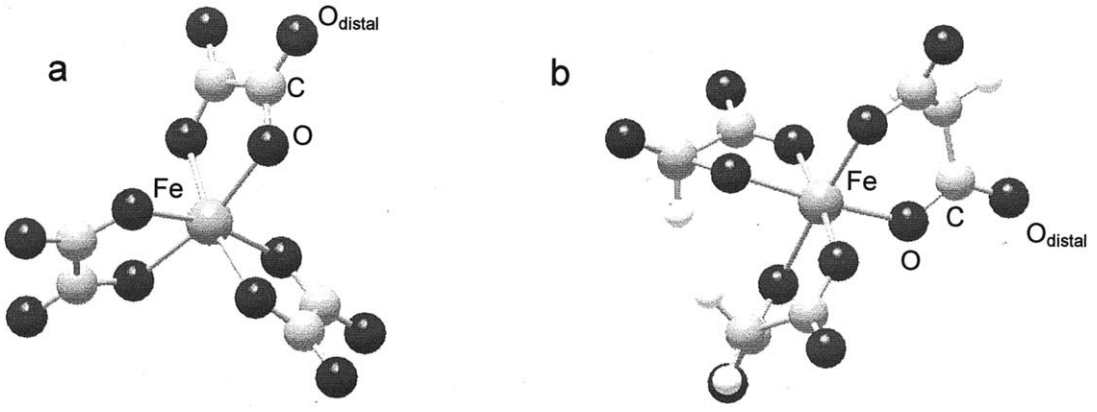

Fig. 2. Structures of (a) $Fe(C_2O_4)_3^{3-}$ and (b) $Fe(H_2C_3O_4)_3^{3-}$ obtained from the DFT geometry optimizations.

Table 3. EXAFS fit results of Fe(III) complexes with oxalate and malonate.

	$Fe(C_2O_4)_3^{3-}$				$Fe(H_2C_3O_4)_3^{3-}$			
Path	N	R (Å)	σ^2	ΔE_0	N	R (Å)	σ^2	ΔE_0
Fe—O	5.9	2.02 (2.04)	0.0086	3.8	6.1	2.02 (2.04)	0.0082	4.2
Fe—C	5.9	2.82 (2.87)	0.0056	3.8	6.1	2.97 (3.03)	0.0077	4.2
Fe—O—C#	11.8	3.06	0.0120	3.8	12.2	3.12	0.0426	4.2
Fe—C	—	—	—	—	3.1	3.26 (3.29)	0.0064	4.2
$Fe—O_{distal}$	5.9	4.03 (4.05)	0.0029	3.8	6.1	4.18 (4.20)	0.0095	4.2
Fe—C—O#	11.8	4.04	0.0061	3.8	12.2	4.22	0.0084	4.2
Fe—C—O—C#	11.8	4.08	0.0077	3.8	—	—	—	—
Fe—O—O#	11.8	4.15	0.0148	3.8	12.2	4.22	0.0123	4.2

S_0^2 was fixed at 1. Values in parentheses are distances from the DFT optimized structures.
Energy shift, ΔE_0, was allowed to vary, but kept internally constant for all shells within a particular complex.
Uncertainties in R are estimated in the first shell to ±0.02 Å and in the higher order shells to ±0.04 Å.
Uncertainties in coordination numbers are estimated to at least ±20%.
MS paths correlated to single scattering coordination numbers and distances, and angles fixed to values of the structures used in the FEFF calculations.

amplitude functions for fitting the experimental data. The paths to be included in the fits were selected from the most important single scattering contributions and multiple scattering contributions as predicted by the FEFF calculations (see Fig. 2; Table 3). Thus, the fit results presented below will reveal structural similarities and differences between the DFT optimized structures and the solution complexes. To keep the number of fit parameters as low as possible, no multiple scattering paths from the first coordination shell were included. The coordination numbers, distances, and Debye-Waller factors for the single scattering contributions were free variables in the fits, whereas the coordination numbers and the distances of the multiple scattering paths were correlated to the corresponding single scattering contributions. In none of the data fits was the Brillouin-Nyquist limit on the number of free variables ($N_{free} = 2\Delta r_{filtered}\Delta k/\pi$) exceeded (Brillouin, 1962). This fitting approach provided a very good fit to data, and the models are presented in Figure 1 and Table 3.

First shell fits revealed close to six oxygen back-scatterers at a distance of 2.02 Å for both complexes. Also, the Debye-Waller factors were very similar. These observations show that the bonding, as viewed by EXAFS spectroscopy, between Fe(III) and the two ligands is practically identical and any differences in the thermodynamic stabilities of the two complexes is probably not due to differences in the local bonding between Fe(III) and the oxygen atoms.

The higher order shells are satisfactorily modeled by single-scattering paths from the carbon atoms and the distal oxygens, in combination with multiple scattering contributions involving the coordinated oxygens, the distal oxygens, and the carbon atoms of the ligand (cf. Figs. 1 and 2; Table 3). The main differences between the two systems are the Fe-C single scattering contribution from the additional central carbon atom of malonate, and the need to include a four-legged Fe-C-O-C multiple-scattering path to fit the higher shells of the Fe(III)-oxalate complex. The reason why this multiple scattering path is needed to fit the oxalate system only is believed to be due to the geometry of the five-membered chelate ring structure. This structure makes the $Fe-C-O_{distal}$ path more linear than in the malonate complex, and thus increases the significance of multiple scattering through these atoms. As seen in Table 3, the distances obtained from the EXAFS analysis are in close agreement with those in the DFT structures. This, together with the coordination numbers of Fe-C and $Fe-O_{distal}$, show that both oxalate and malonate coordinate with the expected chelate structures depicted in Figure 2.

In accordance with these findings, the theoretical IR spectra of the DFT optimized structures are in reasonable agreement with the experimental IR spectra of $Fe(C_2O_4)_3^{3-}$ and $Fe(H_2C_3O_4)_3^{3-}$ (Fig. 3), considering that solution effects have been neglected in the calculations. Since the theoretical vibrational modes are known, we can by direct comparison tentatively assign the experimental frequencies (Tables 4a and 4b). These assignments are in good agreement with those previously suggested (Öhrström and Michaud-Soret, 1999), and provide explanations to the observed spectral changes when the deprotonated ligands are transferred from a hydrated state to a Fe(III)-coordinated chelating state (Tables 2a and b and 4a and b). From these assignments it is also clear that the intense C-O stretching vibrations constitute distinct indicators for both ligands in these two structural environments. Finally, the close similarity between IR spectra of FeL^+ and FeL_3^{3-} (L = oxalate or malonate) is noteworthy. This similarity implies that most probably the ligands retain the chelating structure in all of the aqueous $FeL_n^{(3-2n)}$ complexes, which has previously been shown to be the case for the corresponding Ga(III) and Al(III) complexes (Clausén et al., 2003).

3.2. Characterization of Surface Complexes

The main objectives of the IR-spectroscopic measurements were to study how the IR spectral characteristics of adsorbed oxalate and malonate change with pH and ligand concentration to determine the number of surface complexes and their coordination modes to the goethite surface. Both systems were studied at total ligand concentrations of 0.7 and 1.4 μmol per m^2 of goethite. The IR spectra at these two concentrations were very similar in appearance, and therefore, only the 1.4 μmol/m^2 results will be discussed in this section. In the quantitative evaluation presented below, however, results from both total concentrations will be used.

In a previous study of oxalate adsorbed on boehmite, the distribution of surface species was shown to vary with time (Axe and Persson, 2001), and 10 to 15 h of reaction were

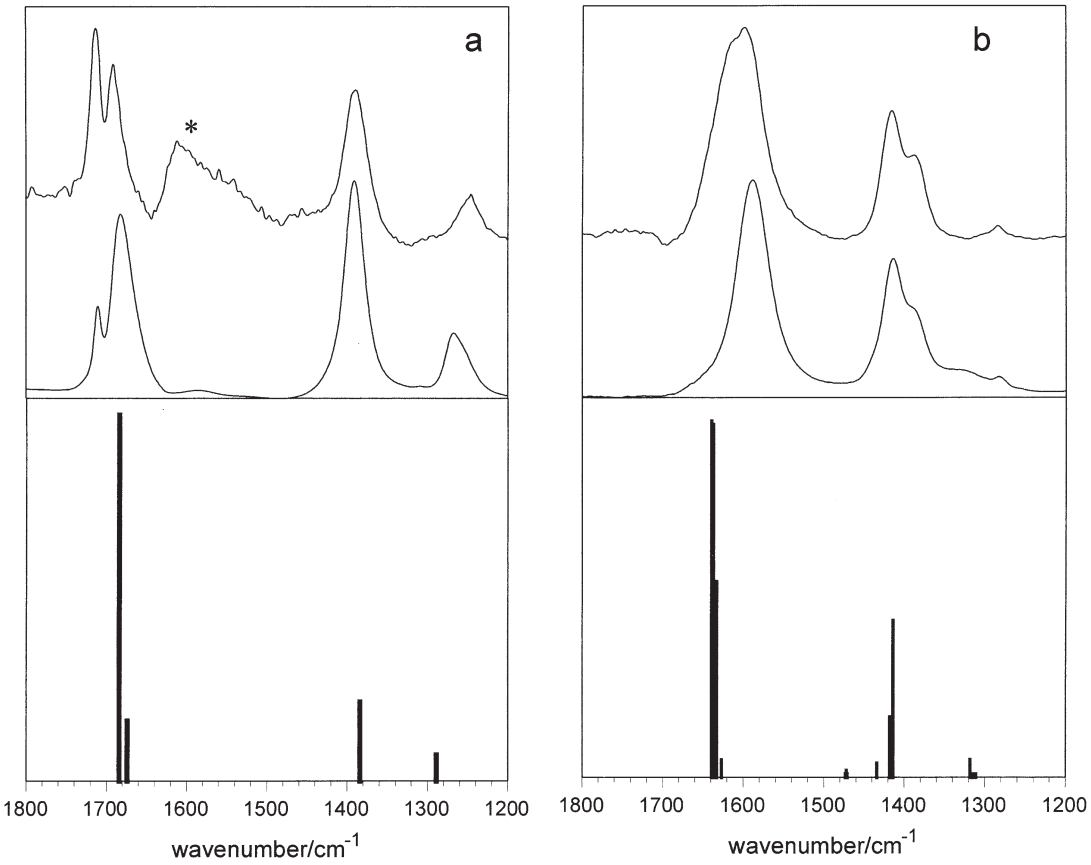

Fig. 3. ATR-FTIR spectra of FeL^{+} (upper spectrum) and FeL_3^{3-} (lower spectrum) where (a) L = oxalate, and (b) L = malonate. Included are also the theoretical IR spectra of FeL_3^{3-} from the DFT calculations. *This band is assigned to the bending mode of the four coordinated water molecules needed to complete the octahedral structure of FeL^{+} (aq).

needed to reach steady state. In contrast, time-resolved measurements of the systems studied herein showed that steady state was attained after 2 h of reaction. All results presented below were obtained after 24 h of reaction, and thus represent equilibrium or pseudoequilibrium conditions.

3.2.1. Identification of oxalate surface complexes

When oxalate adsorbs to goethite, prominent peaks occur at 1713, 1692, 1590, 1404 (at pH 2.7; gradually increasing to 1427 at pH 6.8), 1307, and 1255 cm^{-1} (Fig. 4). Going from low to higher pH, an increase in the relative importance of the 1590 and 1307 cm^{-1} peaks is observed, suggesting that the surface speciation is pH dependent and that more than one surface species is formed. To confirm this, the IR spectrum at the highest pH was subtracted from those at lower pH values, and vice versa. Differences in the amount of adsorbed oxalate were corrected for by adjusting the subtraction factor accordingly. This subtraction procedure resulted in two sets of very different IR-spectroscopic features, showing the presence of two structurally different surface complexes and confirming that the distribution between these two surface species is pH dependent (Fig. 5).

Table 4a. Main experimental and theoretical IR frequencies of Fe(III)-oxalate complexes.

	$\nu_{C-O}{}^{nb}$	$\nu_{C-O}{}^{nb}$	$\nu_{C-O}{}^{b} + \nu_{C-C}$	$\nu_{C-O}{}^{b} + \delta_{O-C-O}$
$Fe(C_2O_4)^{+}$ (e)	1713	1691	1389	1246
$Fe(C_2O_4)_3^{3-}$ (e)	1710	1683	1392	1267, 1252#
$Fe(C_2O_4)_3^{3-}$ (t)	1684	1674	1384	1289

The assignments of the experimental frequencies are based on the results from the theoretical frequency calculations.
(e) experimental frequencies.
(t) theoretical frequencies.
Shoulder, resolved in second derivative spectrum.
[nb] the oxygen of the carboxylate group not bonded to Fe(III).
[b] the oxygen of the carboxylate group bonded to Fe(III).

Table 4b. Main experimental and theoretical IR frequencies of Fe(III)-malonate complexes.

	$\nu_{C—O}{}^{nb}$	$\nu_{C—O}{}^{b} + \nu_{C—C} + \delta_{CH2}$
$Fe(H_2C_3O_4)^+$ (e)	1610, 1599	1416, 1389, 1285
$Fe(H_2C_3O_4)_3^{3-}$ (e)	1588	1414, 1390, 1283
$Fe(H_2C_3O_4)_3^{3-}$ (t)	1639, 1637, 1633	1418, 1414, 1318

The assignments of the experimental frequencies are based on the results from the theoretical frequency calculations.
(e) experimental frequencies.
(t) theoretical frequencies.
[nb] denotes the oxygen of the carboxylate group not bonded to Fe(III).
[b] denotes the oxygen of the carboxylate group bonded to Fe(III).

3.2.2. Structural assignment of oxalate surface complexes

Subtracting the spectrum of the pH 2.7 sample from spectra of samples prepared at higher pH results in residuals at 1582 and 1307 cm^{-1}, which is in close agreement with the spectrum of $C_2O_4^{2-}$ (aq) ($\nu^{as}_{C\text{-}O}$ at 1569 and $\nu^{as}_{C\text{-}O}$ at 1308 cm^{-1}) (Fig. 5). This shows that the immediate surroundings of oxalate have not changed significantly upon adsorption, and is thus indicative of outer-sphere complexation (Axe and Persson, 2001). However, the full width at half maximum (FWHM) of the 1582 and 1307 cm^{-1} peaks has increased significantly in comparison with the solution spectrum, a phenomenon that can be attributed to a range of slightly different states, including all adsorbed oxalate except those ions directly coordinated to Fe(III). Thus, this encompasses both oxalate ions with an intact hydration shell, and ions which are partly desolvated and hydrogen bonded to surface hydroxyl groups and surface coordinated water molecules. This latter bonding mode is thought to be the cause of the shift of the $\nu_{C\text{-}O}{}^{as}$ from 1569 cm^{-1} in solution to 1582 cm^{-1} at the surface. The collective term HBSC (hydrogen bonded surface complex) will be used for the outer-sphere types of surface complexes.

Subtracting the spectrum of the pH 7.8 sample from the spectra of samples prepared at lower pH values results in residuals with peaks at 1710, 1690, 1400 (exact wavenumber pH dependent), and 1255 cm^{-1}, which is very similar to the spectrum of aqueous $Fe(C_2O_4)^+$ (Fig. 5). This strong resemblance suggests that oxalate, in addition to HBSC, also forms inner-sphere surface complexes with a structure similar to that of $Fe(C_2O_4)^+$ (aq), and hence, complexes with a mononuclear five-membered ring chelate structure. A broadening of the 1400 cm^{-1} peak with 14 cm^{-1} was observed, which might indicate heterogeneity of the inner-sphere sites. Since direct bonds between structural Fe(III) and oxalate are formed, this surface species will be referred to as MBSC (metal-bonded surface complex) in the following discussion.

At the low end of the pH range investigated, a substantial amount of the oxalate in solution is in the monoprotonated form (pK_{a1} = 0.97, pK_{a2} = 3.57) (Smith and Martell, 1982), and thus, conditions exist for formation of protonated surface complexes. As indicated in Table 2a, the strong $\nu_{C=O}$ peak around 1735 cm^{-1} and the equally strong $\nu_{C\text{-}OH}$ peaks around 1233 cm^{-1} are very good indicators for protonation of the oxalate molecule. Neither of these features were observed in the IR spectra of oxalate adsorbed on goethite, and we conclude that no protonated outer-sphere surface species are formed at detectable concentrations under the conditions studied.

3.2.3. Identification of malonate surface complexes

Figure 6 shows IR spectra of malonate adsorbed on goethite as a function of pH at a total ligand concentration of 1.4 $\mu mol/m^2$. Strong peaks are seen around 1580, 1430, and 1340 cm^{-1}, and a weaker one at 1258 cm^{-1}. The relative intensity of the 1340 cm^{-1} peak, compared to that at 1430 cm^{-1}, increases with increasing pH. Concurrent with this change is the shift of the broad band from 1582 cm^{-1} at pH 2.8 to around 1560 cm^{-1} at pH 7.5. These observations show the existence of at least two predominating surface complexes, but the changes are less obvious than in the oxalate system and require further investigation.

To study the spectral features and changes in more detail, the second-derivative spectra were calculated. Derivative spectra usually have sharper features and can be used to reduce the effect of overlapping bands. Thus, calculating the derivatives is a mathematical way of apparently enhancing the resolution. One problem is that the derivative procedure emphasizes narrow features, including noise, and an appropriate interval of data points for the calculation of the derivatives must therefore be chosen, in order not to overemphasize the noise. Another problem is that depending on the shape of the peaks, the derivative spectra might show slight variability of the peak positions compared to the original spectra. This is especially true for broad features containing several overlapping peaks. In second derivatives, sharp negative minima are expected where there are positive maxima in the original spectrum. Therefore, to make the comparison to the original spectra easier, the inverted (around the *x*-axis) second-derivative spectra are presented.

The inverted second-derivative spectra of malonate adsorbed on goethite as a function of pH are presented in Figure 7. These spectra show some features independent of pH, but also distinct differences. Throughout the pH range studied (pH 2.8–8), sharp maxima occur at 1431 and 1258 cm^{-1}. The 1431 cm^{-1}

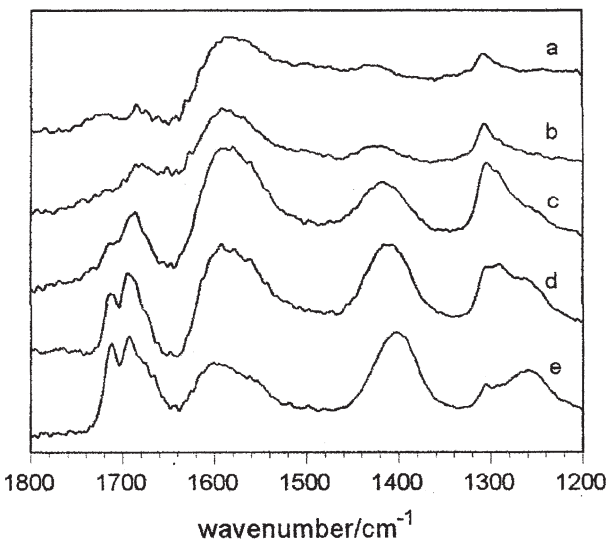

Fig. 4. ATR-FTIR spectra of oxalate adsorbed at the water-goethite interface at pH (a) 7.8, (b) 6.8, (c) 5.3, (d) 4.7, and (e) 2.7, at a total oxalate concentration of 1.4 $\mu mol/m^2$.

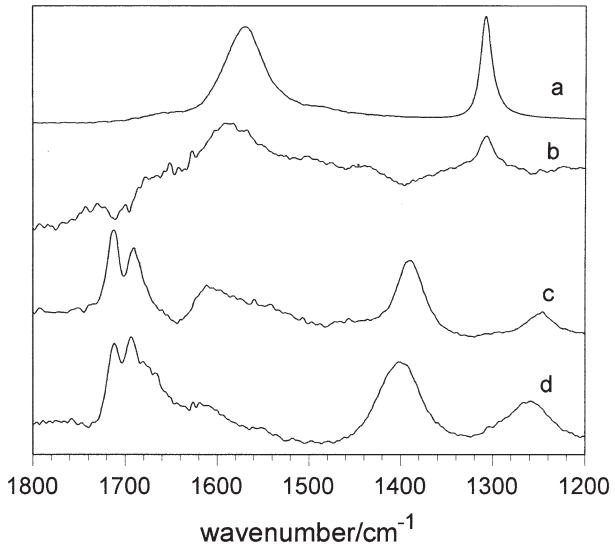

Fig. 5. (a) ATR-FTIR spectrum of $C_2O_4^{2-}$ (aq); (b) difference spectrum obtained by subtracting spectrum Figure 4e (pH 2.7) from spectrum Figure 4a (pH 7.8); (c) ATR-FTIR spectrum of $Fe(C_2O_4)^+$ (aq); and (d) difference spectrum obtained by subtracting spectrum Figure 4a (pH 7.8) from spectrum Figure 4e (pH 2.7). The subtraction procedure is described in the text.

is asymmetric, suggesting that a second and strongly overlapping peak is present. Around 1340 cm^{-1}, the shape and the position of the second-derivative peaks vary with pH. It is clear, however, that at least two peaks are present, and that the high frequency component predominates at high pH while the low frequency peak is most prominent at low pH. The large peak around 1580 cm^{-1} is resolved into two peaks at high pH. As pH is lowered, the separation between the two peaks seems to decrease, although these shifts might be an artifact of the derivative calculations. At low pH, one peak becomes strongly dominating, and at pH below 4, only one maximum is observed at 1581 cm^{-1}. These variations with pH show that the broad peaks at 1580 and 1340 cm^{-1} consist of more than one spectral feature, whose relative distribution is strongly pH dependent, which suggests that they originate from different surface complexes.

To confirm the presence of different surface complexes and their characteristic features, again the spectral subtraction method was used. Subtracting the 2.8 pH spectrum from those at higher pH results in residuals at 1551, 1343, and 1258 cm^{-1}, while subtracting the pH 7.6 spectrum from those at lower pH gives peaks at 1586, 1423, and 1315 cm^{-1}. These two different sets of spectral features obtained (shown in Fig. 8) confirm that (as suggested by the original spectra and second derivatives) two predominating surface complexes of malonate can be identified under the conditions studied.

3.2.4. Structural assignments of malonate surface complexes

The first surface complex (Fig. 8b), whose relative importance increases with increasing pH, absorbs intensely at 1550 and 1343 cm^{-1} and less so at 1256 cm^{-1}, which is very similar to the $\nu_{C\text{-}O}$ peaks in the IR spectrum of $H_2C_3O_4^{2-}$ (aq). This shows that there is no direct bond between malonate and Fe(III), and consequently these spectral features are ascribed to the presence of a HBSC. At the surface, these peaks are broadened and slightly shifted to lower wavenumbers. Thus, the overall behavior is very similar to that of HBSC of oxalate, and the suggested explanations for the peak broadening most probably are valid also for the malonate surface complexes. One difference between oxalate and malonate, however, is the direction of the small peak shifts as compared to the aqueous species. The reason to this is not clear, but since the actual vibration modes are slightly different (see Tables 2a and 2b) the analysis is difficult to make without extensive molecular orbital calculations.

The second complex (Fig. 8d), present under all conditions investigated here and becoming more important at low pH, shows strong peaks at 1586 cm^{-1}, 1422 cm^{-1}, (asymmetric) and a weaker one at 1316 cm^{-1}. When comparing this to the solution spectra, all the features from $Fe(H_2C_3O_4)^+$ (aq) are found, which implies inner-sphere complexation to Fe(III). The 1416 cm^{-1} in the aqueous complex has broadened and shifted 8 cm^{-1} towards higher wavenumbers, resulting in the broad and asymmetric peak at 1422 cm^{-1}, of which 1382 cm^{-1} is a component, as shown in the second-derivative spectra. On the other hand, the $\nu_{C\text{-}O}{}^{nb}$ at 1600 cm^{-1} in solution has shifted 16 cm^{-1} downwards to 1584 cm^{-1} in the surface complex. This means that the split between $\nu^{nb}_{C\text{-}O}$ and $\nu^{b}_{C\text{-}O}$ has decreased 24 cm^{-1} as compared to the solution complex, which might indicate a slightly weaker interaction with the surface (Deacon and Phillips, 1980; Persson et al., 1998). Despite the shifts in frequencies, the overall IR characteristics of $Fe(H_2C_3O_4)^+$ (aq) and the surface complex are very similar, and accordingly, the structure of the MBSC is suggested to be a six-membered chelate ring.

Because of the relatively high pK_a values of malonic acid (pK_{a1} = 2.65, pK_{a2} = 5.28) (Smith and Martell, 1982), conditions are more favorable for formation of protonated surface complexes than in the oxalate system. However, the absence of

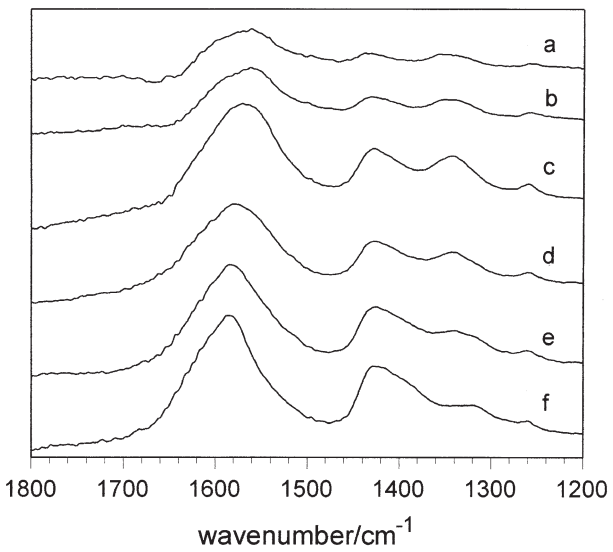

Fig. 6. ATR-FTIR spectra of malonate adsorbed at the water-goethite interface at pH (a) 7.6, (b) 6.7, (c) 5.5, (d) 4.8, (e) 3.8, and (f) 2.8, at a total malonate concentration of 1.4 $\mu mol/m^2$.

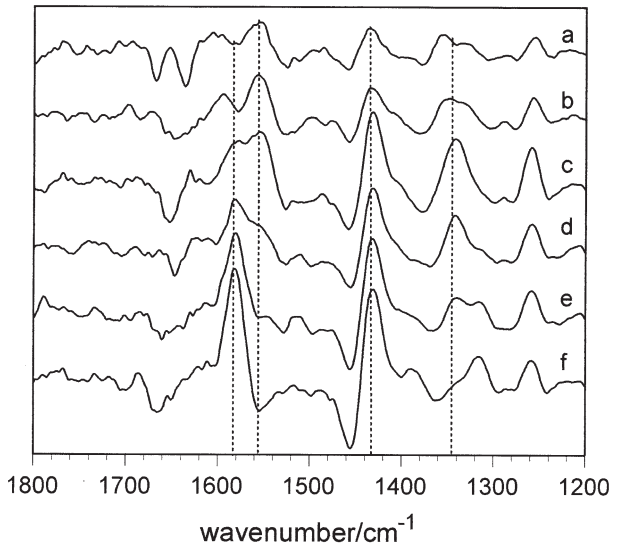

Fig. 7. The inverted second-derivative ATR-FTIR spectra of the malonate-goethite interface at pH (a) 7.6, (b) 6.7, (c) 5.5, (d) 4.8, (e) 3.8, and (f) 2.8, at a total malonate concentration of 1.4 μmol/m^2.

the peaks corresponding to $\nu_{C=O}$ and $\nu_{C\text{-}OH}$ (see Fig. 6; Table 2b) again shows that no protonated outer-sphere surface complexes form under the conditions studied herein.

Overall, in comparison with previous studies our results are in good agreement with those of malonate adsorbed on hematite presented by Lenhart et al. (2001).

3.3. Quantitative Evaluation of the Molecular-Level Surface Speciation

The discussion above has shown that the distribution between MBSC and HBSC of oxalate and malonate is strongly pH dependent. To gain further insight about the pH dependent surface speciation, IR spectra were evaluated in a semiquantitative manner to estimate the actual concentrations of the different surface complexes.

The method to quantitatively evaluate the IR spectra has been described in a previous publication (Axe and Persson, 2001) and relies on the similar appearance of the spectra of $C_2O_4^{2-}/H_2C_3O_4^{2-}$ (aq) and $Fe(C_2O_4)^+/Fe(H_2C_3O_4)^+$ (aq) and their surface counterparts HBSC and MBSC, respectively. By recording IR spectra for L^{2-} and FeL^+ solutions (L = oxalate or malonate) at different concentrations, the molar absorption coefficients (ε) of the observed peaks can be determined. Though the absolute ε-values of the solution complexes and the surface complexes may differ, it is likely that the ratio of ε for two particular peaks should be approximately similar for the solution and the surface species. Thus, by determining the ε ratio from the solutions, analyzing the areas of the corresponding peaks of the surface complexes, and knowing the total ligand adsorption, the absolute surface concentration of the individual surface complexes can be calculated from IR spectroscopy data. Note that this approach relies on the similarity of vibrations between solution and surface complexes. If the vibrational modes are significantly different, then the probability of absorption of infrared radiation will also be different and the method will fail.

The 1308 cm^{-1} ($C_2O_4^{2-}$), 1357 cm^{-1} ($H_2C_3O_4^{2-}$), 1390 cm^{-1} ($Fe(C_2O_4)^+$), and 1416 + 1383 cm^{-1} ($Fe(H_2C_3O_4)^+$) peaks were selected for the quantitative evaluation, and the absorptivities were determined from solutions containing 5 to 20 mM to 0.0137, 0.0085, 0.0101, and 0.0169 A^2/M, respectively, using linear regression. Thus, the corresponding $\varepsilon_L/\varepsilon_{FeL}$ ratios were 1.4 and 0.5 for the oxalate and malonate systems. Assuming that the ε ratios are the same for the corresponding peaks characterizing the HBSC and MBSC, and by combining the equations:

$$C_{HBSC} + C_{MBSC} = C_{tot}$$

$$C_{HBSC}/C_{MBSC} = (\varepsilon_{FeL}/\varepsilon_L)(A_{HBSC}/A_{MBSC})$$

where C_{HBSC} is the surface concentration of HBSC, C_{MBSC} is the surface concentration of MBSC, C_{tot} is the total surface concentration (as measured by liquid scintillation counting), A_{HBSC} and A_{MBSC} are the HBSC and MBSC selected peak areas, expressions for calculating the surface concentration of the individual complexes can be derived:

$$C_{MBSC} = C_{tot}/(1 + (\varepsilon_{FeL}/\varepsilon_L)(A_{HBSC}/A_{MBSC}))$$

$$C_{HBSC} = C_{tot} - C_{tot}(1 + (\varepsilon_{FeL}/\varepsilon_L)(A_{HBSC}/A_{MBSC}))$$

Evaluation of the IR peak areas was accomplished using the curve-fitting program PeakFit version 4 (SPSS Inc.). To evaluate the robustness of this procedure, three series of batch experiments with similar total malonate concentrations of 0.6, 0.7, and 0.8 μmol/m^2 covering a wide range of pH (2.5–8) were used. The same fitting procedure was applied to all spectra, and by comparing the obtained surface concentrations

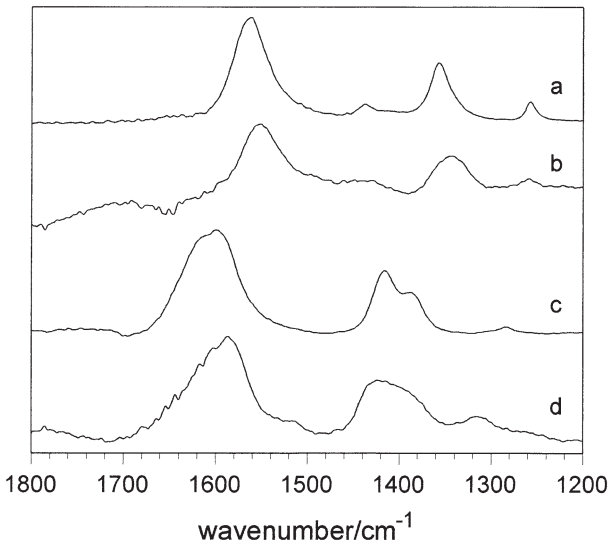

Fig. 8. (a) ATR-FTIR spectrum of $H_2C_3O_4^{2-}$ (aq); (b) difference spectrum obtained by subtracting spectrum Figure 6f (pH 2.8) from spectrum Figure 6a (pH 7.6); (c) ATR-FTIR spectrum of $Fe(H_2C_3O_4)^+$; and (d) difference spectrum obtained by subtracting spectrum Figure 6a (pH 7.6) from spectrum Figure 6f (pH 2.8). The subtraction procedure is described in the text.

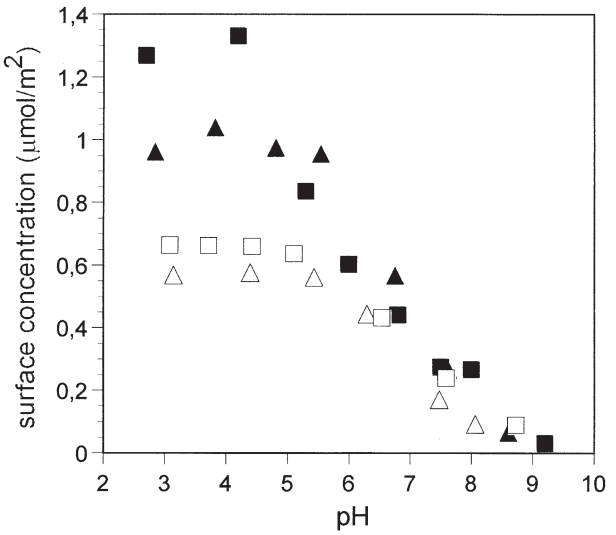

Fig. 9. Surface concentration on goethite as a function of pH at total oxalate concentrations 0.7 μmol/m^2 (□) and 1.4 μmol/m^2 (■), and total malonate concentrations of 0.7 μmol/m^2 (△) and 1.4 μmol/m^2 (▲).

at each pH value and assuming that the surface speciation is not affected by the slight variation in total ligand concentration, the errors in HBSC/MBSC ratios were less than 5% up to pH around 6.5. At higher pH, where very small amounts of malonate adsorb, the uncertainty increased to ~20% due to the small peaks obtained.

Figure 9 shows the surface concentration of oxalate and malonate as a function of pH at total ligand concentrations of 0.7 and 1.4 μmole/m^2. At both ligand concentrations, the amounts of adsorbed oxalate and malonate are rather constant in the pH 3 to 5.5 range. With further increasing pH, the surface concentration decreases rapidly, and when pH approaches the isoelectric point (IEP) of goethite (~ 9.4), the surface concentrations become negligible (Hiemstra et al., 1996). Between pH 6 and 8.5, the adsorbed amounts for both ligands are very similar. At low pH, however, the adsorption curves differ, especially at high total concentrations where significantly more oxalate is adsorbed. This implies an overall stronger oxalate-surface interaction in the acidic pH range.

When the total surface concentrations are recalculated into the individual fractions of HBSC and MBSC, additional details are revealed that explain the difference in adsorption behavior between oxalate and malonate (Fig. 10). The most significant results are the increased importance of HBSC for malonate and MBSC for oxalate. By comparing Figures 9 and 10, it follows that the enhancement of oxalate adsorption is due to the formation of MBSC. Based on the structural assignments of MBSC of oxalate and malonate, we can ascribe this stability increase to the five-membered ring structure of oxalate. Thus, the trend in MBSC stabilities with ring structure seems to follow that of solution complexes (Smith and Martell, 1982).

Finally, it is of interest to compare the HBSC/MBSC ratios as a function of pH and total ligand concentration. These ratios also reveal significant differences between the oxalate and malonate systems (Fig. 11). While the oxalate ratios show pH and concentration dependence, the HBSC/MBSC ratios of malonate at 0.7 and 1.4 μmol/m^2 total concentrations are very similar (Fig. 11). Thus, within this concentration interval, the malonate HBSC/MBSC ratio does not seem sensitive to the total amount of malonate adsorbed.

4. CONCLUSIONS

The results presented herein show that oxalate and malonate both form outer-sphere and inner-sphere surface complexes on goethite, and that these complexes coexist over a broad pH range. Hence, even though these are comparatively strong complex-forming ligands in aqueous solution, outer-sphere species need to be considered in their surface complexation reactions. The inner-sphere complexes are favored by low pH, while the relative concentrations of the outer-sphere species increase with increasing pH. Based on comparisons with well-characterized model complexes and results from theoretical frequency calculations, the inner-sphere complexes of oxalate and malonate are assigned mononuclear five- and six-mem-

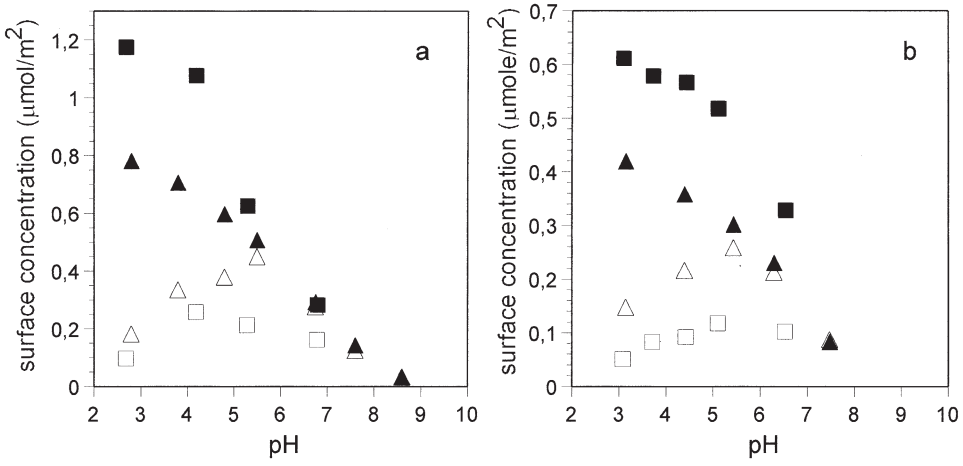

Fig. 10. Surface concentrations of oxalate MBSC (■), oxalate HBSC (□), malonate MBSC (▲), and malonate HBSC (△) as a function of pH at total oxalate and malonate concentrations of (a) 1.4 μmol/m^2 and (b) 0.7 μmol/m^2.

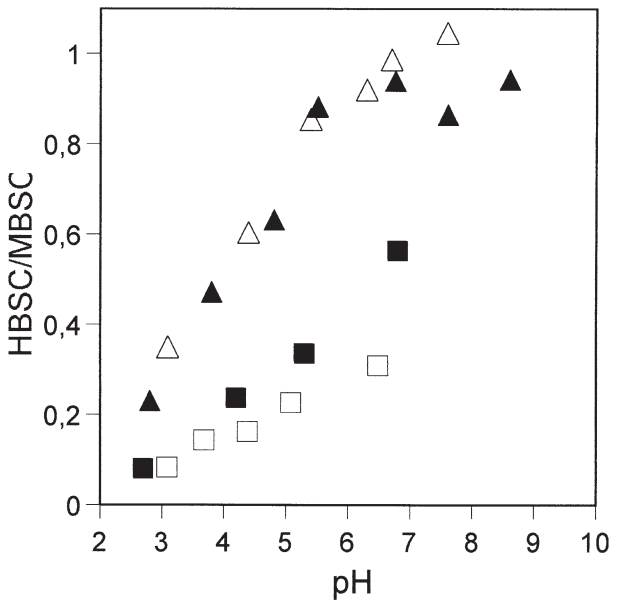

Fig. 11. The HBSC/MBSC ratio as a function of pH at total oxalate concentrations 0.7 μmol/m^2 (□) and 1.4 μmol/m^2 (■), and total malonate concentrations of 0.7 μmol/m^2 (△) and 1.4 μmol/m^2 (▲).

bered ring chelate structures, respectively. The stability of the inner-sphere complexes follows the trend expected from studies of aqueous oxalate and malonate iron(III) complexes with the five-membered ring yielding the more stable complexes. The increased stability of the inner-sphere complex of oxalate is manifested in a greater extent of adsorption at acidic pH values. As no significant increase in soluble Fe was observed, an important conclusion from this study is that formation of oxalate and malonate inner-sphere complexes do not necessarily promote a fast dissolution of goethite. At the experimental conditions used, these inner-sphere surface complexes are indicated to be stable with respect to dissolution and formation of soluble iron(III)-ligand complexes.

Acknowledgments—We would like to thank Ms. Åsa Gustafsson and Ms. Marie Vejgården for help with the IR measurements and Prof. Staffan Sjöberg for valuable suggestions and comments. We thank the staff of Stanford Synchrotron Radiation Laboratory (SSRL), particularly Prof. Britt Hedman and Dr. John Bargar, for their help and advice. SSRL is operated by the Department of Energy, Office of Basic Energy Sciences. We also acknowledge the National Institutes of Health, National Center for Research Resources, Biomedical Technology Program, and the Department of Energy Office of Biologic and Environmental Research, which support the SSRL Structural Molecular Biology Program whose instrumentation was used for the measurements. This work was supported by the Swedish Research Council and The Swedish Foundation for International Cooperation in Research and Higher Education (STINT).

Associate editor: C. Eggleston

REFERENCES

Ali A. M. and Dzombak D. A. (1996) Competitive sorption of simple organic acids and sulfate on goethite. *Environ. Sci. Technol.* **30,** 1061–1071.

Ankudinov A. L., Ravel B., Rehr J. J., and Conradson S. D. (1998) Real-space multiple-scattering calculation and interpretation of x-ray-absorption near-edge structure. *Phys. Rev. B.* **58,** 7565–7576.

Axe K. and Persson P. (2001) Time-dependent surface speciation of oxalate at the water-boehmite (γ-AlOOH) interface: implications for dissolution. *Geochim. Cosmochim. Acta* **65,** 4481–4492.

Balistrieri L. S. and Murray J. W. (1987) The influence of the major ions in seawater on the adsorption of simple organic acids by goethite. *Geochim. Cosmochim. Acta* **51,** 1151–1160.

Bell J. L. S. and Palmer D. A. (1994) Experimental studies of organic acid decomposition. In *Organic Acids in Geological Processes* (ed. E. D. Pittman and M. D. Lewan), Springer-Verlag, pp. 226–269.

Bennett P. C. and Casey W. (1994) Chemistry and mechanisms of low-temperature dissolution of silicates by organic acids. In *Organic Acids in Geological Processes* (ed. E. D. Pittman and M. D. Lewan), Springer-Verlag, pp. 162–200.

Boily J.-F., Nilsson N., Persson P., and Sjöberg S. (2000) Benzenecarboxylate surface complexation at the goethite (α-FeOOH)/water interface: II. Linking IR spectroscopic observations to mechanistic surface complexation models for phthalate, trimellitate and pyromellitate *Geochim. Cosmochim. Acta* **64,** 3453–3470.

Brillouin L. (1962) *Science and Information Theory* 2nd Edition, Academic Press.

Cabaniss S. E., Leenheer J. A., and McVey I.-F. (1998) Aqueous infrared carboxylate absorbances: aliphatic di-acids. *Spectrochim. Acta A.* **54,** 449–458.

Clausén M., Öhman L.-O., Axe K., and Persson P. (2003) Spectroscopic studies of aluminum and gallium complexes with oxalate and malonate in aqueous solution. *J. Mol. Struct.* **648,** 225–235.

Deacon G. B. and Phillips R. J. (1980) Relationships between the carbon-oxygen stretching frequencies of carboxylato complexes and the type of carboxylate coordination. *Coord. Chem. Rev.* **33,** 227–250.

Dobson K. D. and McQuillan A. J. (1999) In situ infrared spectroscopic analysis of the adsorption of aliphatic carboxylic acids to TiO_2, ZrO_2, Al_2O_3 and Ta_2O_5 from aqueous solutions. *Spectrochim. Acta A.* **55,** 1395–1405.

Drever J. I. and Vance G. F (1994) Role of soil organic acids in mineral weathering processes. In *Organic Acids in Geological Processes* (ed. E. D. Pittman and M. D. Lewan), Springer-Verlag, pp. 138–161.

Duckworth O. D. and Martin S. T. (2001) Surface complexation and dissolution of hematite by C_1-C_6 dicarboxylic acids at pH = 5.0 *Geochim. Cosmochim. Acta* **65,** 4289–4301.

Eriksson G. (1979) An algorithm for the computation of aqueous multicomponent, multiphase equilibria. *Anal. Chim. Acta* **112,** 375–383. (For further information see http://www.chem.umu.se/dep/inorgchem/).

Filius J. D., Hiemstra T., and Van Riemsdijk W. H. (1997) Adsorption of small weak organic acids on goethite: modeling of mechanisms. *J. Colloid Interface Sci.* **195,** 368–380.

Frisch M. J., Trucks G. W., Schlegel H. B., Scuseria G. E., Robb M. A., Cheeseman J. R., Zakrzewski V. G., Montgomery Jr. J. A., Stratmann R. E., Burant J. C., Dapprich S., Millam J. M., Daniels A. D., Kudin K. N., Strain M. C., Farkas O., Tomasi J., Barone V., Cossi M., Cammi R., Mennucci B., Pomell, C., Adamo C., Clifford S., Ochterski J., Petersson G. A., Ayala P. Y., Cui Q., Morokuma N., Rega P., Salvador J. J., Dannenberg D. K., Malick A. D., Rabuck K., Raghavachari K., Foresman J. B., Cioslowski J., Ortiz J. V., Baboul A. G., Stefanov B. B., Liu G., Liashenko A., Piskorz P., Komaromi I., Gomperts R., Martin R. L., Fox D. J., Keith T., Al-Laham M. A., Peng C. Y., Nanayakkara A., Challacombe M., Gill P. M. W., Johnson B., Chen W., Wong M. W., Andres J. L., Gonzalez C., Head-Gordon M., Replogle E. S., and Pople J. A. (2001) Gaussian 98. Revision A. 11.2, Gaussian, Inc.

George G. N (1995) EXAFSPAK. Stanford Synchrotron Radiation Laboratory.

Hiemstra T., Venema P., and van Riemsdijk W. H. (1996) Intrinsic Proton affinity of reactive surface groups of metal (hydr)oxides: the bond valence principle. *J. Colloid Interface Sci.* **184,** 680–692.

Hind A. R., Bhargava S. K., and McKinnon A. (2001) At the solid/liquid interface: ATR/FTIR the tool of choice. *Adv. Coll. Interface Sci.* **93,** 91–114.

Hug S. J. and Sulzberger B. (1994) In situ Fourier transform infrared spectroscopic evidence for the formation of several different surface complexes of oxalate on TiO_2 in the aqueous phase. *Langmuir* **10,** 3587–3597.

Johansson G. (1992) Structures of complexes in solution derived from x-ray diffraction measurements. *Adv. Inorg. Chem.* **39,** 159–231.

Kubicki J. D., Schroeter L. M., Itoh M. J., Nguyen B. N., and Apitz S. E. (1999) Attenuated total reflectance Fourier-transform infrared spectroscopy of carboxylic acids adsorbed onto mineral surfaces. *Geochim. Cosmochim. Acta* **63,** 2709–2725.

Kummert R. and Stumm W. (1980) The surface complexation of organic acids on hydrous γ-Al_2O_3. *J. Colloid Interface Sci.* **75,** 373–385.

Lenhart J. J., Bargar J. R., and Davis J. A. (2001) Spectroscopic evidence for ternary surface complexes in the lead(II)-malonic acid-hematite system. *J. Colloid Interface Sci.* **234,** 448–452.

Lützenkirchen J., Boily J.-F., Lövgren L., and Sjöberg S. (2002) Limitations of the potentiometric titration technique in determining the proton active site density of goethite surfaces. *Geochim. Cosmochim. Acta* **66,** 3389–3396.

Martell A. E. and Hancock R. D. (1996) *Metal Complexes in Aqueous Solution* Chapter 3. Plenum Press.

Mesuere K. and Fish W. (1992) Chromate and oxalate adsorption on goethite. 1. Calibration of surface complexation models *Environ. Sci. Technol.* **26,** 2357–2364.

Nordin J., Persson P., Laiti E., and Sjöberg S. (1997) Adsorption of *o*-phthalate at the water-boehmite (γ-AlOOH) interface: evidence for two coordination modes. *Langmuir* **13,** 4085–4093.

Öhrström L. and Michaud-Soret I. (1999) Fe-catecholate and Fe-oxalate vibrations and isotopic substitution shifts from DFT quantum chemistry. *J. Phys. Chem. A.* **103,** 256–264.

Parfitt R. L., Farmer V. C., and Russell J. D. (1977) Adsorption on hydrous oxides. I. Oxalate and benzoate on goethite. *J. Soil Sci.* **28,** 29–39.

Persson P., Karlsson M., and Öhman L.-O. (1998) Coordination of acetate to Al(III) in aqueous solution and at the water-aluminum hydroxide interface: a potentiometric and attenuated total reflectance FTIR study. *Geochim. Cosmochim. Acta* **62,** 3657–3658.

Ressler T. (1998) WinXAS: a program for X-ray absorption spectroscopy data analysis under MS-Windows. *J. Synch. Rad.* **5,** 118–122.

Rosenqvist J., Axe K., Sjöberg S., and Persson P. (2003) Adsorption of dicarboxylates on nano-sized gibbsite particles: effects of ligand structure on bonding mechanisms. *Colloids and Surfaces A.* **220,** 91–104.

Smith R. M. and Martell A. E (1982) *Critical Stability Constants,* Volume 5: First Supplement. Plenum.

Stumm W. (1992) *Chemistry of the Solid-Water Interface.* John Wiley & Sons, Inc..

Tejedor-Tejedor M. I., Yost E. C., and Anderson M. A. (1992) Characterization of benzoic and phenolic complexes at the goethite/aqueous solution interface using cylindrical internal reflection fourier transform infrared spectroscopy. 2. Bonding structures. *Langmuir* **8,** 525–533.

Urban M. W. (1996) *Attenuated Total Reflectance of Polymers*. American Chemical Society.

Yost E. C., Tejedor-Tejedor M. I., and Anderson M. A. (1990) In situ CIR-FTIR characterization of salicylate complexes at the goethite/aqueous solution interface. *Environ. Sci. Technol.* **24,** 822–828.